PERGAMON

International Journal of Solids and Structures 36 (1999) 1209–1229

INTERNATIONAL JOURNAL OF SOLIDS and STRUCTURES

Deflections and buckling of a bent elastica in contact with a flat surface

Raymond H. Plaut[a,*], Surjani Suherman[a], David A. Dillard[b], Brad E. Williams[b], Layne T. Watson[c]

[a]*The Charles E. Via, Jr. Department of Civil Engineering, Virginia Polytechnic Institute and State University, Blacksburg, VA 24061, U.S.A.*

[b]*Department of Engineering Science and Mechanics, Virginia Polytechnic Institute and State University, Blacksburg, VA 24061, U.S.A.*

[c]*Departments of Computer Science and Mathematics, Virginia Polytechnic Institute and State University, Blacksburg, VA 24061, U.S.A.*

Received 18 June 1997; in revised form 27 October 1997

Abstract

A straight elastica is bent until its ends are vertical and a fixed distance apart, and then it is pushed onto a flat rigid surface. The weight of the strip and friction between the strip and the surface are neglected. Planar equilibrium states of the strip are investigated, using either a shooting method or an integral formulation. Both symmetric and asymmetric configurations are possible. There may be a single point of contact, a flat region of contact, or two points of contact with a buckled section between them. Also, if the ends are pushed down sufficiently far, one or two loops may form when the upper portion of the strip makes contact with the lower portion on the surface. If the two ends are held together (vertically) and then pushed down, asymmetric configurations may occur in which there is a region of contact between the upper and lower portions of the strip near their ends. The properties of these various equilibrium shapes are investigated.

1. Introduction

A thin, uniform, horizontal, inextensible, flexible strip is considered. The ends of the strip are lifted, bent, and clamped vertically at an equal height and a specified distance apart, as shown in Fig. 1. Then the ends are moved downward and the strip makes contact with a flat, rigid, horizontal surface. Various planar equilibrium shapes are possible, including: symmetric with a single contact point as in Fig. 2(a); symmetric with a flattened region as in Fig. 2(b); symmetric with two contact

* Corresponding author.

0020–7683/99/$ - see front matter
PII: S0020–7683(97)00348–X

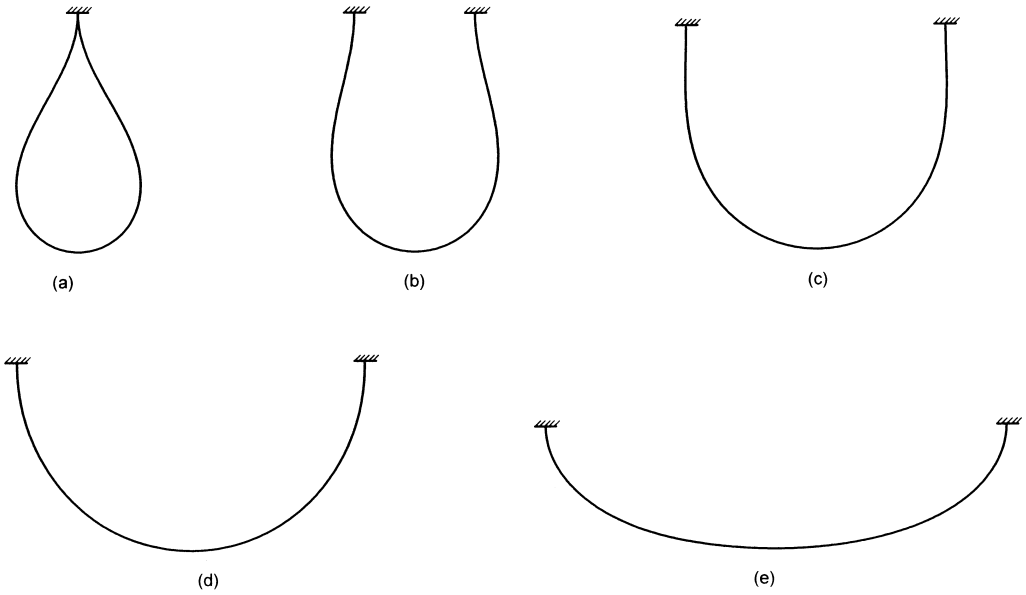

Fig. 1. Equilibrium shapes before contact: (a) $c = 0$; (b) $c = 0.2$; (c) $c = 0.4$; (d) $c = 0.6$; (e) $c = 0.8$.

points and a buckled region as in Figs 2(c) and 2(d); symmetric with two outer loops as in Fig. 2(e); asymmetric with a single contact point as in Fig. 2(f); asymmetric with a flattened region as in Fig. 2(g); and asymmetric with a flattened region and a loop as in Fig. 2(h). Tick marks in Fig. 2 indicate points of contact or lift-off of the lower portion of the strip with the surface, and the scales are different in each part of the figure.

Some related problems have been treated in the literature. Wang (1981) analyzed an elastica bent between two horizontal surfaces, with each end of the elastica tangential to one of the surfaces. Iseki et al. (1989a, b) considered a curved strip, with pinned or clamped ends, that was compressed by a flat plate. The strip was extensible, and only symmetric deformations were studied. Experimental results were presented, as well as numerical results obtained with the finite element method. The transition from the flattened to the buckled configuration could occur smoothly or suddenly (snap-through). In Grigolyuk and Shalashilin (1991), the same type of problem was examined numerically for an elastic circular arch with pinned ends.

Compression of an inflated spherical membrane by parallel rigid plates was analyzed by Feng and Yang (1973) and Evans and Skalak (1980). Similar studies involving shells include Wang (1987) for cylindrical tubes (and rings), Mack et al. (1983) and Sugita (1985) for toroidal shells, and Kinkead et al. (1994) and Nowinka and Lukasiewicz (1994) for spherical shells. The shells are flattened by the plates and in some cases buckle inward with a profile of the form in Fig. 1(c). These investigations have been related to the denting of vehicles, ships, and submarines (Kitching et al., 1975), the deformations of tires (Mack et al., 1983), the testing of pressure on the cornea (Updike and Kalnins, 1972), and the adhesion of vesicles and red blood cells to surfaces (Evans, 1980).

In this paper, the strip is assumed to be elastic and inextensible, and the bending moment is

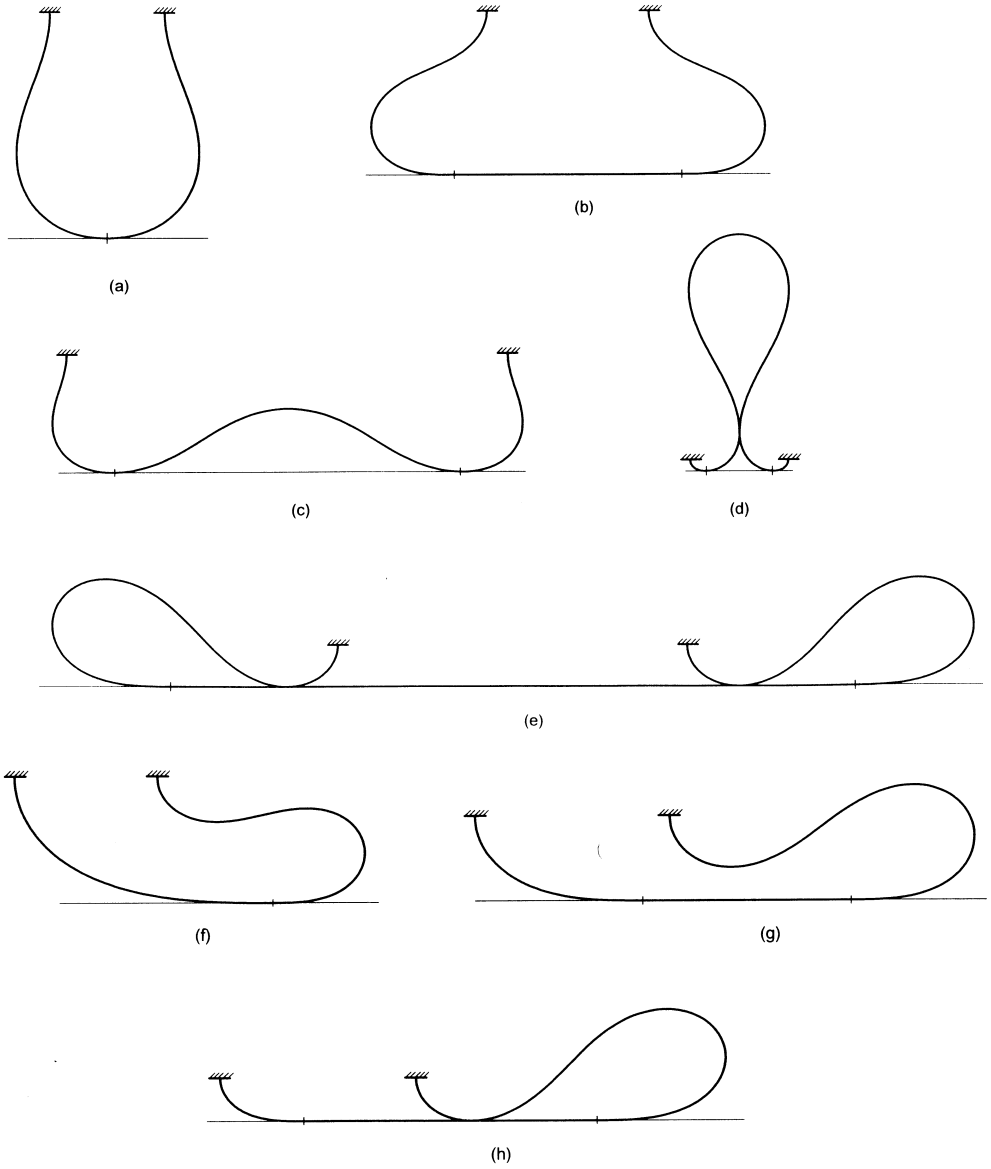

Fig. 2. Some equilibrium shapes: (a) symmetric with point contact; (b) symmetric with line contact; (c) symmetric with buckled region; (d) symmetric and buckled with self-contact; (e) symmetric with two loops; (f) asymmetric with point contact; (g) asymmetric with line contact; (h) asymmetric with loop.

assumed to be proportional to the curvature, i.e., the strip is an elastica (Gorski, 1976). The weight of the strip is neglected, and friction between the strip and the rigid surface also is neglected. Equilibrium shapes are analyzed. Numerical solutions are obtained using either a shooting method or a formulation involving integrals. As the strip is pushed down onto the flat surface, the variations of the contact region and the forces and moments at the ends of the strip are determined.

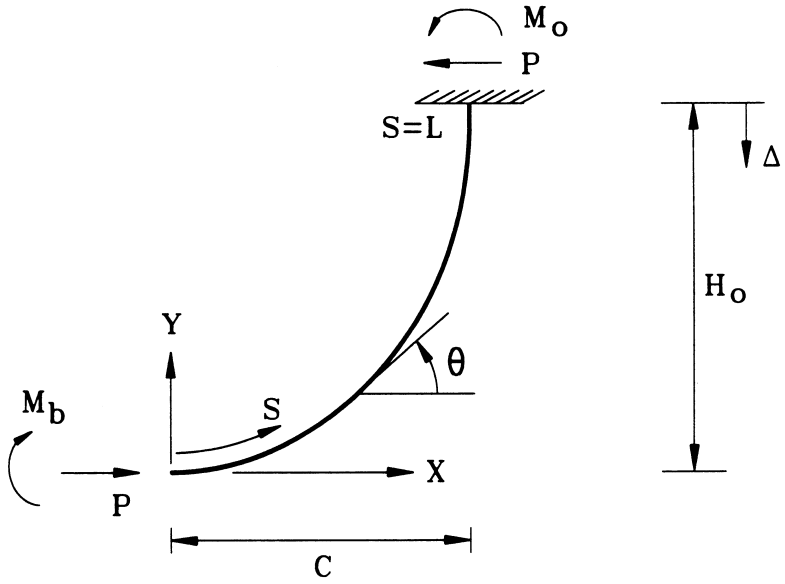

Fig. 3. Free body diagram of right half of strip before contact.

2. No contact

Equilibrium shapes, before contact occurs, are considered first. The length of the strip is $2L$ and the bending stiffness is EI. The initially-straight elastica is bent until its ends are a distance $2C$ apart at a fixed height, and the ends are clamped with vertical slopes. The right half of the strip is drawn in Fig. 3. The origin of the coordinate system is placed at the bottom where the slope is zero. The arc length is S, the angle of the tangent with the horizontal is θ, and the horizontal and vertical coordinates are X and Y, respectively. The constant horizontal force is P and the variable bending moment is M, with $M = M_b$ at $S = 0$ and $M = M_o$ at $S = L$. Positive senses are as shown in Fig. 3.

From geometry, the moment–curvature relation, and equilibrium of an element, the governing equations are

$$\frac{dX}{dS} = \cos\theta, \quad \frac{dY}{dS} = \sin\theta, \quad EI\frac{d\theta}{\theta S} = M, \quad \frac{dM}{dS} = -P\sin\theta. \tag{1a,b,c,d}$$

The known end conditions are $X = Y = \theta = 0$ at $S = 0$, and $X = C$, $\theta = \pi/2$ at $S = L$ where the height is denoted $Y(L) = H_o$ for this no-contact case.

The following nondimensional quantities are introduced:

$$x = X/L, \quad y = Y/L, \quad s = S/L, \quad h_o = H_o/L, \quad h = H/L,$$
$$b = B/L, \quad c = C/L, \quad d = D/L, \quad \delta = \Delta/L, \quad m = ML/(EI), \quad m_b = M_bL/(EI),$$
$$m_o = M_oL/(EI), \quad p = PL^2/(EI), \quad q = QL^2/(EI), \quad u = UL/(EI) \tag{2}$$

where H, B, D, Δ, Q, and U will be defined later. In nondimensional form, the governing eqns (1a–d) become

$$\frac{dx}{ds} = \cos\theta, \quad \frac{dy}{ds} = \sin\theta, \quad \frac{d\theta}{ds} = m, \quad \frac{dm}{ds} = -p\sin\theta \tag{3a,b,c,d}$$

with $x = y = \theta = 0$ at $s = 0$, and $x = c$, $\theta = \pi/2$ at $s = 1$.

For a specified value of c, (3a–d) are solved with a shooting method (Wolfram, 1991; Bahder, 1995). Values of $m(0)$ and p are guessed, the equations are integrated numerically until $s = 1$, and these values are then varied using the secant method or Brent's method until the end conditions at $s = 1$ are satisfied with sufficient accuracy. The nondimensional height h_o is given by $y(1)$. (Alternatively, if c need not be specified, one can vary p until $\theta = \pi/2$ at $s = 1$, and then c is the obtained value of x at $s = 1$.)

Another type of solution procedure in terms of integrals is also available. Eqns (3c,d) lead to

$$\frac{d\theta}{\theta s} = \pm\frac{1}{\rho} \tag{4a}$$

where

$$\rho = 1/\sqrt{2p(g + cos\theta)} \tag{4b}$$

and g is a constant. When there is no inflection point (i.e., when m_o turns out to be positive), the positive sign is used in (4a). Then, using (3a, b, 4a, b) and integrating, one can show that

$$s = \int_0^\theta \rho\, d\theta, \quad x = \int_0^\theta \rho\cos\theta\, d\theta, \quad y = \sqrt{\frac{2}{p}}(\sqrt{g+1} - \sqrt{g+\cos\theta}). \tag{5a,b,c}$$

If the integration is carried out till the right end of the strip, these equations become

$$1 = \int_0^{\pi/2} \rho\, d\theta, \quad c = \int_0^{\pi/2} \rho\cos\theta\, d\theta, \quad h_o = \sqrt{\frac{2}{p}}(\sqrt{g+1} - \sqrt{g}). \tag{6a,b,c}$$

If c is specified, one can solve (6a, b) numerically for g and p (Bahder, 1995), and then determine h_o from (6c). If not, one can vary g and compute p, c, and h_o directly from (6a–c). The case $g = 0$ gives c = 0.457.

For $c < 0.457$, there is an inflection point on each half of the strip. If the value of θ at the inflection point on the right half is denoted α, (6a–c) are replaced by

$$1 = \int_0^\alpha \rho\, d\theta - \int_\alpha^{\pi/2} \rho\, d\theta, \quad c = \int_0^\alpha \rho\cos\theta\, d\theta - \int_\alpha^{\pi/2} \rho\cos\theta\, d\theta,$$

$$h_o = \int_0^\alpha \rho\sin\theta\, d\theta - \int_\alpha^{\pi/2} \rho\sin\theta\, d\theta, \tag{7a,b,c}$$

where ρ is given in (4b) with $g = -\cos\alpha$ (since the bending moment is zero at the inflection point). For a given value of c, (7a, b) are solved numerically for α and p, and h_o is determined from (7c).

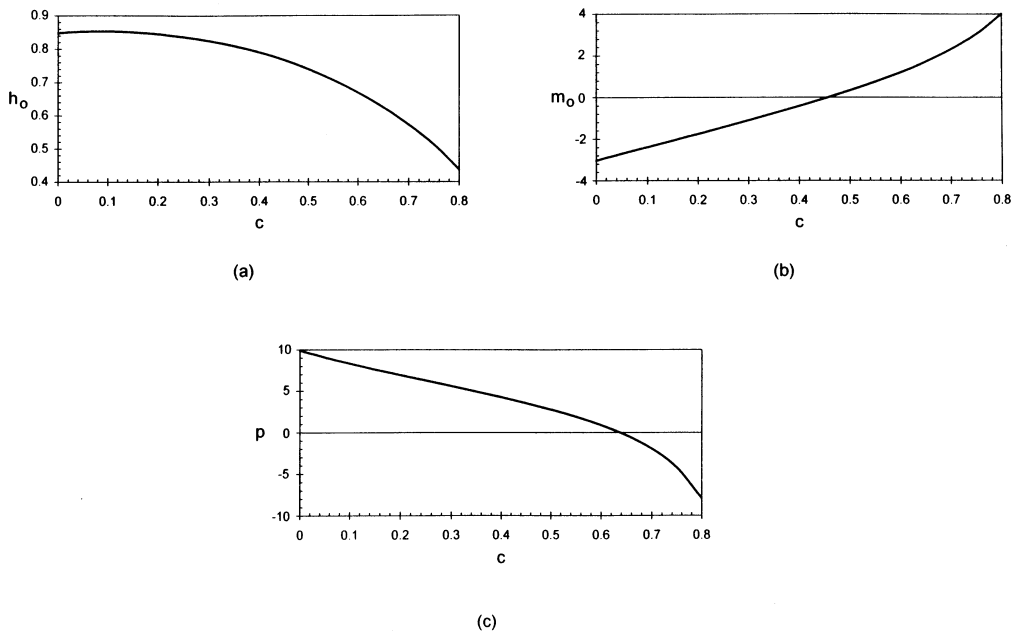

Fig. 4. Effect of separation length of ends on: (a) height; (b) end moments; (c) horizontal force.

Once the reactions are known, equilibrium shapes can be determined by numerical integration of the equilibrium equations (3) or from the integral formulation (5). The shapes for $c = 0$, 0.2, 0.4, 0.6, and 0.8 are depicted in Fig. 1. Further results are presented in nondimensional form in Fig. 4 and Table 1. The height h_o, end moment m_o, and horizontal force p are plotted versus the separation parameter c for the range $0 < c < 0.8$ in Fig. 4. As c is increased from 0, the height increases from $h_o = 0.849$ until it reaches 0.853 at $c = 0.09$ and then decreases, the horizontal forces act inward until $c = 0.637 = 2/\pi$ (when the shape is circular), and the moment at the right end is counter-clockwise until $c = 0.457$. The moment m_b at the bottom ($s = 0$) can be obtained by equilibrium (Fig. 3).

Table 1
No contact (O)

c	h_o	p	m_o
0	0.849	9.91	−3.03
0.2	0.845	6.93	−1.75
0.4	0.790	4.26	−0.415
0.6	0.668	0.879	1.20
0.8	0.437	−7.93	4.02

The solution for $c = 0$ was previously given by Wang (1981). He obtained the similarity solution

$$s_{\text{loop}} = 6.29688/\sqrt{p}, \quad h_{\text{o}} = 2.67181/\sqrt{p}, \quad m_{\text{o}} = -0.96163\sqrt{p}, \quad m_{\text{b}} = 1.71018\sqrt{p}. \tag{8}$$

where s_{loop} is the nondimensional length of the loop, equal to 2 in this case, and where p and m_{o} act just below the right end of the strip. This solution will be utilized later in the analysis of the central portion of the equilibrium configuration depicted in Fig. 1(d).

3. Symmetric with point contact

Next, assume that the center of the bent strip comes into contact with a flat surface parallel to the line connecting the ends of the strip, as shown in Fig. 2(a). The height of the strip is H, and the downward deflection of the ends relative to the no-contact height is Δ (Fig. 3), so that $\Delta = H_{\text{o}} - H$. (In nondimensional terms, $\delta = h_{\text{o}} - h$ [see eqn (2)].) The right half of the strip is shown in Fig. 5. The downward force on each end is Q, and the upward reaction force at the contact point is therefore $2Q$.

In this case, the governing nondimensional equations are (3a–c) and

$$\frac{\mathrm{d}m}{\mathrm{d}s} = -p\sin\theta + q\cos\theta \tag{9}$$

where q is defined in eqn (2). The end conditions are again $x = y = \theta = 0$ at $s = 0$, and $x = c$, $\theta = \pi/2$ at $s = 1$. The same shooting method described in Section 2 is applied here, with the additional specification of q. The value of q is increased from zero until the bending moment m_{b} at the contact point decreases to zero, at which point the contact zone spreads as detailed in Section 4.

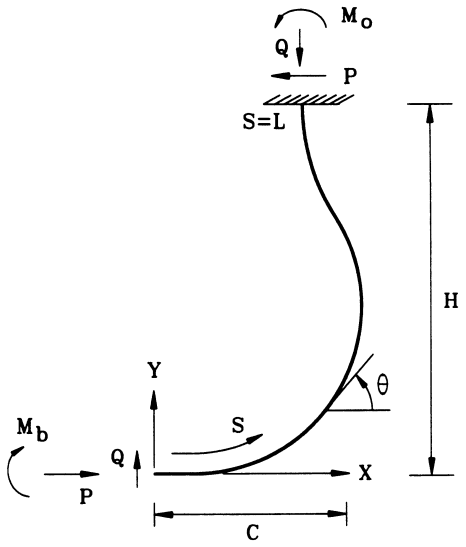

Fig. 5. Free body diagram of right half of strip with symmetric point contact.

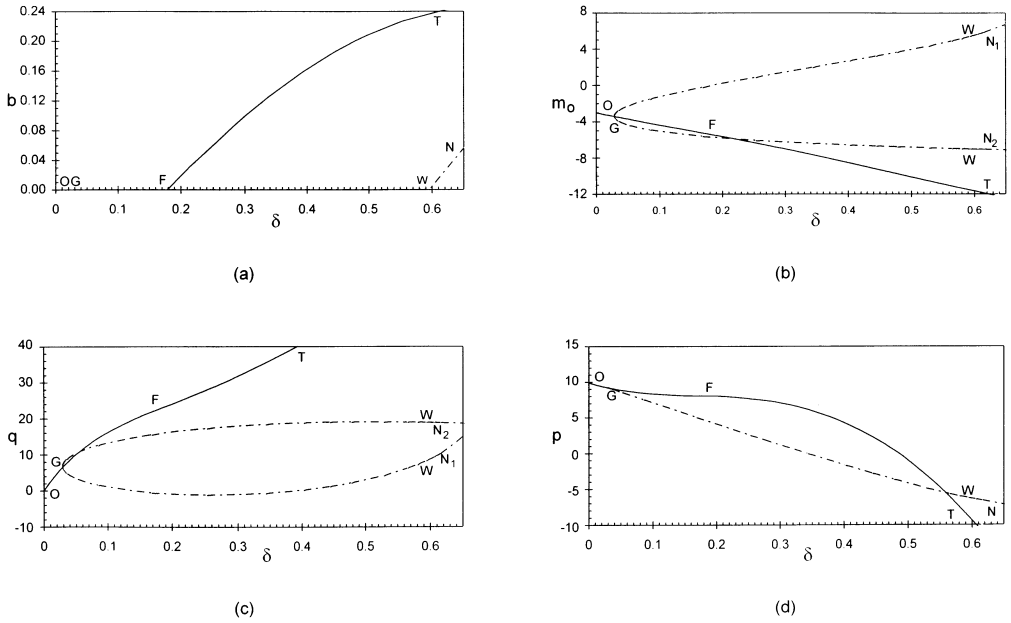

Fig. 6. For $c = 0$, effect of downward displacement on: (a) contact length; (b) moments near end; (c) vertical forces near end; (d) horizontal force in strip.

Results for $c = 0$, 0.2, 0.4, 0.6, and 0.8 are depicted in Figs 6–10, respectively. The quantities b, m_o, q, and p are plotted as functions of the downward deflection δ. Symmetric equilibrium shapes with central point contact are associated with segment OF (on which the contact length parameter b is zero) in these figures. The parameter values at point F, where m_b becomes zero, are listed in Table 2. At F, the equilibrium shapes for $c = 0$, 0.2, 0.4, and 0.6 exhibit inflection points (since $m_o < 0$), while the one for $c = 0.8$ does not. The configuration in Fig. 2(a) corresponds to the case $c = 0.2$ with $\delta = 0.054$.

One can define a "spring constant" for this symmetric downward deflection with central point contact, using the total downward force $2q$ at F divided by the deflection δ at F. In dimensional terms, one obtains the values $253EI/(L^3)$, $267EI/(L^3)$, $259EI/(L^3)$, $230EI/(L^3)$, and $181EI/(L^3)$, respectively, for $c = 0$, 0.2, 0.4, 0.6, and 0.8. The initial "spring constant", computed from twice the slope at O in Figs 6–10, is approximately $517EI/(L^3)$, $449EI/(L^3)$, $379EI/(L^3)$, $306EI/(L^3)$, and $181EI/(L^3)$, respectively.

4. Symmetric with line contact

As the strip is pushed down further, the central region flattens against the surface and there is a line of contact. The unknown length of the flattened region is 2B, as shown in Fig. 11. Figure 5 can be used to illustrate the right part of the strip that is above the surface, except that the horizontal length is now $C-B$ rather than C, and the value of S at the right end is $L-B$ rather

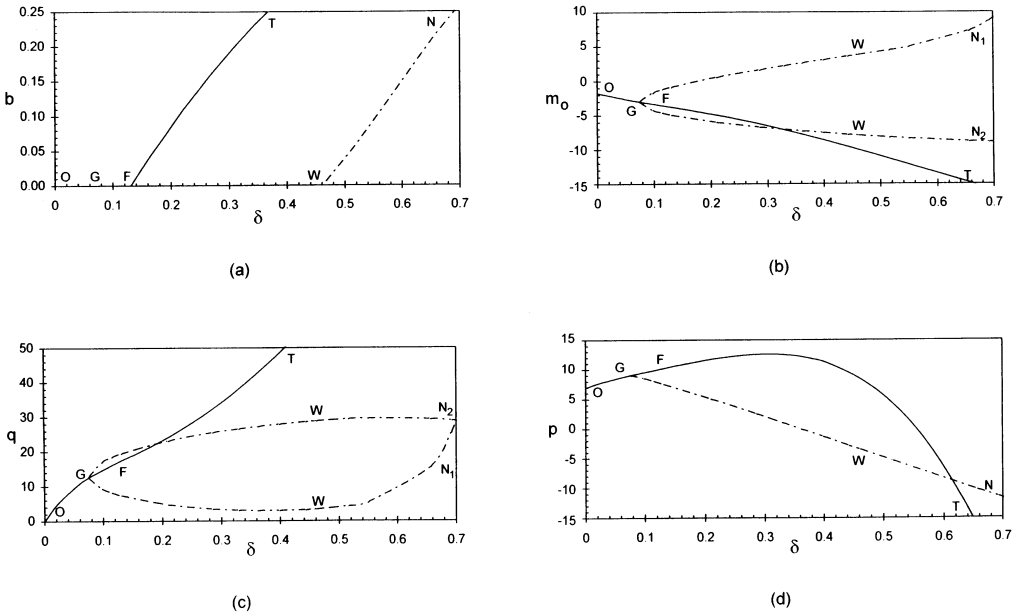

Fig. 7. For $c = 0.2$, effect of downward displacement on (a) contact length; (b) end moments; (c) vertical forces; (d) horizontal force.

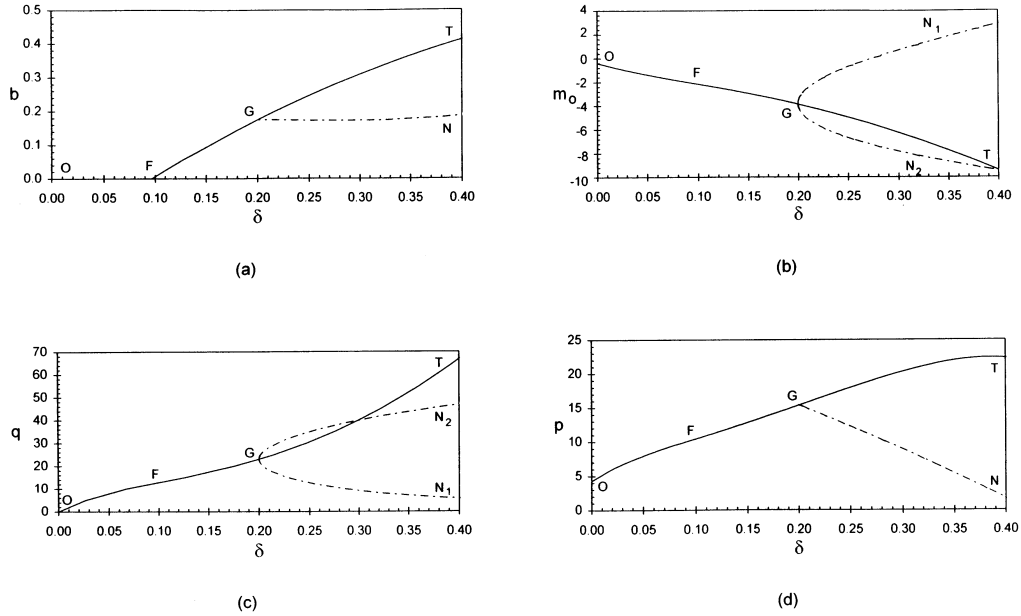

Fig. 8. For $c = 0.4$, effect of downward displacement on: (a) contact length, (b) end moments, (c) vertical forces, (d) horizontal force.

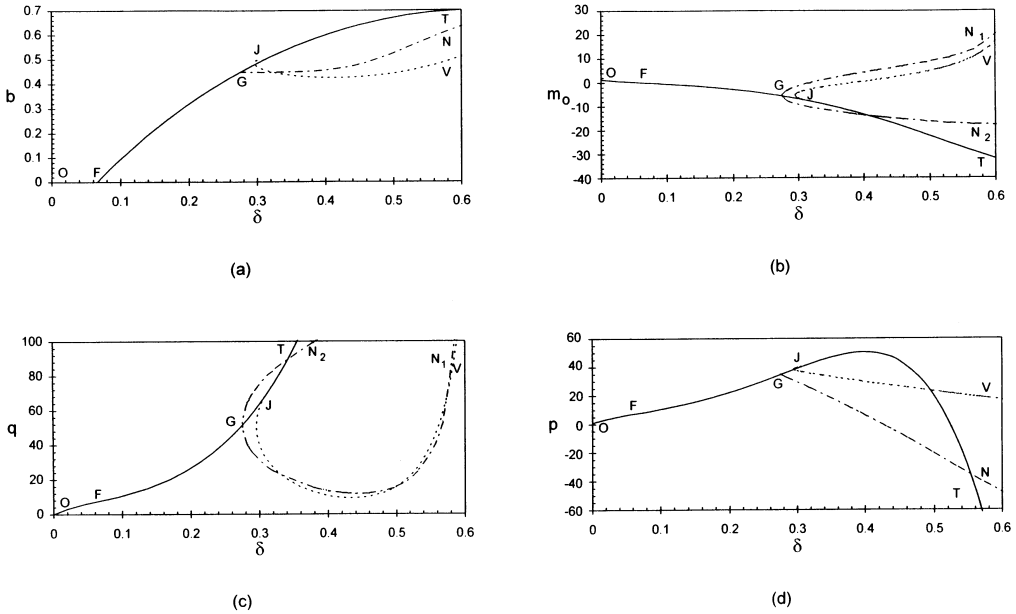

Fig. 9. For $c = 0.6$, effect of downward displacement on: (a) contact length; (b) end moments; (c) vertical forces; (d) horizontal force.

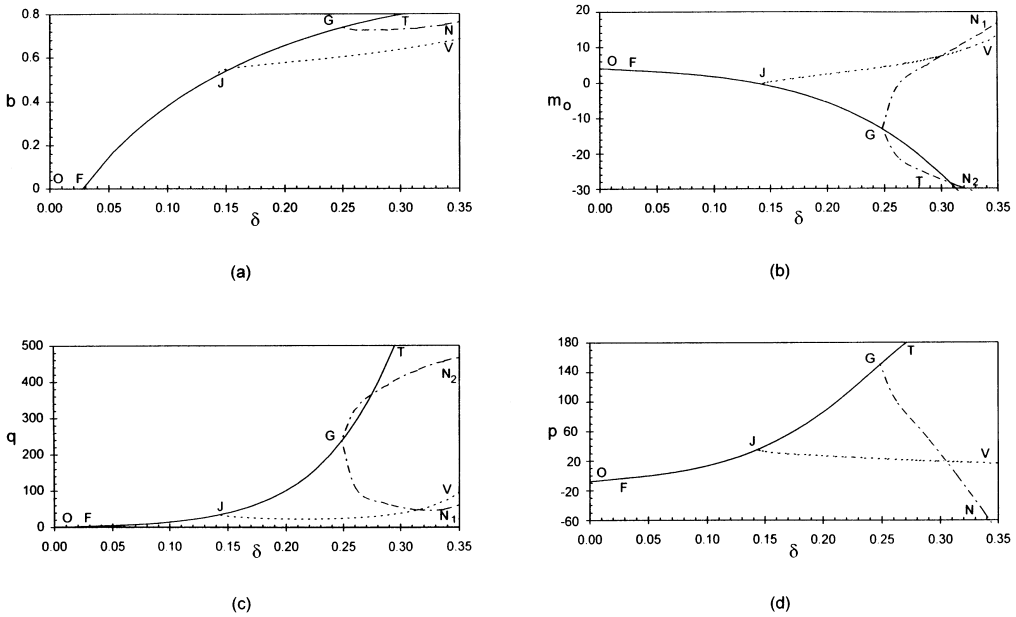

Fig. 10. For $c = 0.8$, effect of downward displacement on: (a) contact length; (b) end moments; (c) vertical forces; (d) horizontal force.

Table 2
Transition from symmetric point contact to symmetric line contact (F)

c	h	δ	q	p	m_o
0	0.670	0.179	22.6	8.05	−5.39
0.2	0.715	0.131	17.4	10.2	−3.80
0.4	0.693	0.0966	12.5	10.3	−2.12
0.6	0.602	0.0659	7.59	7.59	−0.0188
0.8	0.409	0.0275	2.49	−3.79	3.54

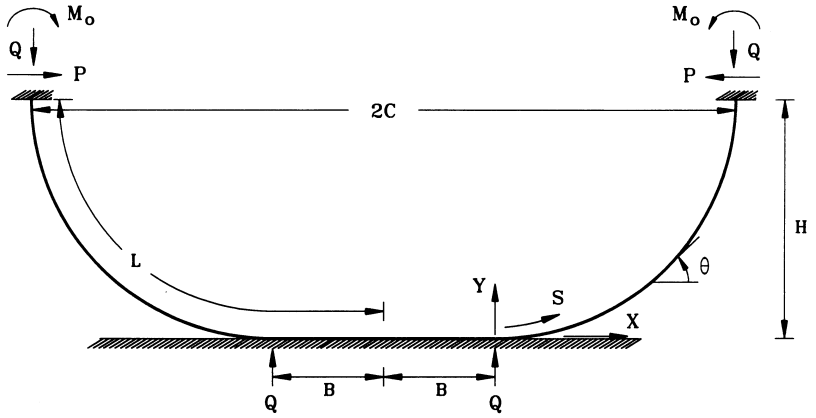

Fig. 11. Geometry of strip for symmetric shape with line contact.

than L. Also, since θ and hence M are zero on the flattened region, and M is continuous at the lift-off point ($S = 0$), $M_b = 0$ in this case.

The governing equations are (3a–c) and (9), with end conditions $x = y = \theta = m = 0$ at $s = 0$, and $x = c-b$, $\theta = \pi/2$ at $s = 1-b$ where b is defined in eqn (2). A scaled arc length z is introduced in this uplifted region as

$$z = s/t \text{ where } t = 1-b. \tag{10a,b}$$

The nondimensional length t is treated as a variable which has a constant value. The governing equations then become

$$\frac{dx}{dz} = t\cos\theta, \quad \frac{dy}{dz} = t\sin\theta, \quad \frac{d\theta}{dz} = tm,$$

$$\frac{dm}{dz} = -tp\sin\theta + tq\cos\theta, \quad \frac{dt}{dz} = 0, \tag{11a,b,c,d,e}$$

and the conditions at the upper end $z = 1$ become $x = c+t-1$ and $\theta = \pi/2$. The system is solved using a shooting method. The separation parameter c is specified and q is set at a value greater

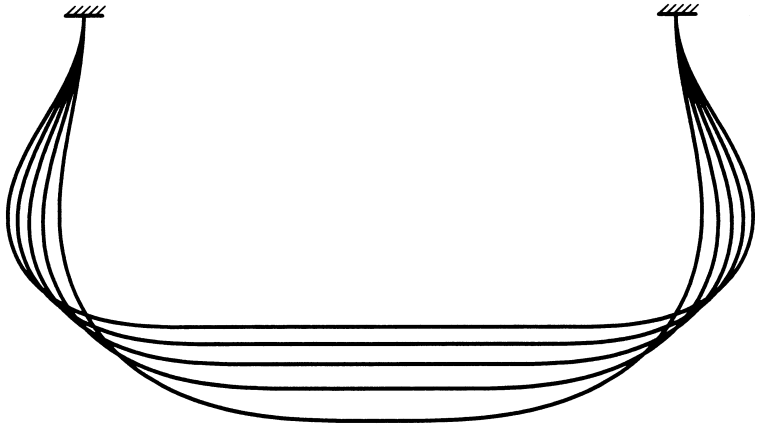

Fig. 12. Sequence of symmetric shapes with line contact ($c = 0.6$).

than the final value from the point-contact case in Section 3. Then values of $t(0)$ and p are varied until the conditions at $z = 1$ are satisfied. Alternatively, a solution procedure in terms of integrals can be derived, using eqn (4a) with

$$\rho = 1/\sqrt{2(p\cos\theta - p + q\sin\theta)}. \tag{12}$$

At the ends of the strip, $\theta = \pi/2$ and one obtains the relation $m_o^2 = 2(q-p)$.

In Figs 6–10, the solid curves from F to T correspond to symmetric equilibrium shapes with line contact. These shapes have inflection points when m_o is negative, which occurs for all cases in Figs 6–10 except when $\delta < 0.135$ for $c = 0.8$. Figure 2(b) depicts the configuration for $c = 0.2$ and $\delta = 0.409$. A sequence of equilibrium shapes for $c = 0.6$ is shown in Fig. 12, with the end points fixed at the same height. The values of δ for these shapes are 0.193, 0.231, 0.260, 0.283, and 0.303, respectively, with corresponding half-lengths b of the flattened region equal to 0.308, 0.378, 0.425, 0.461, and 0.489.

The initial "spring constant" for the downward deflection when the strip begins to flatten (i.e., $2\mathrm{d}q/\mathrm{d}\delta$ at F), in dimensional terms, is approximately $139EI/(L^3)$, $147EI/(L^3)$, $152EI/(L^3)$, $152EI/(L^3)$, and $152EI/(L^3)$, respectively, for $c = 0$, 0.2, 0.4, 0.6, and 0.8. As the strip is pushed down further and the length of the flattened region increases, the spring constant increases (as indicated by the increasing slope on the segments FT in part (c) of Figs 6–10.

5. Symmetric with buckled region

If $c > 0.51$, the flattened region in the symmetric case described in Section 4 can buckle upward as the elastica is pushed down. The case $c = 0.6$ with $\delta = 0.199$ and $b = 0.476$ is shown in Fig. 2(c), where b is half the length between the two contact points. This type of buckling occurs when the compressive force p reaches the value $(\pi/b)^2$, which is the nondimensional critical load for a clamped-clamped column of length $2b$. The critical values of the parameters can be computed by putting $p = [\pi/(1-t)]^2$ in eqn (11d) and using the shooting method described above but with

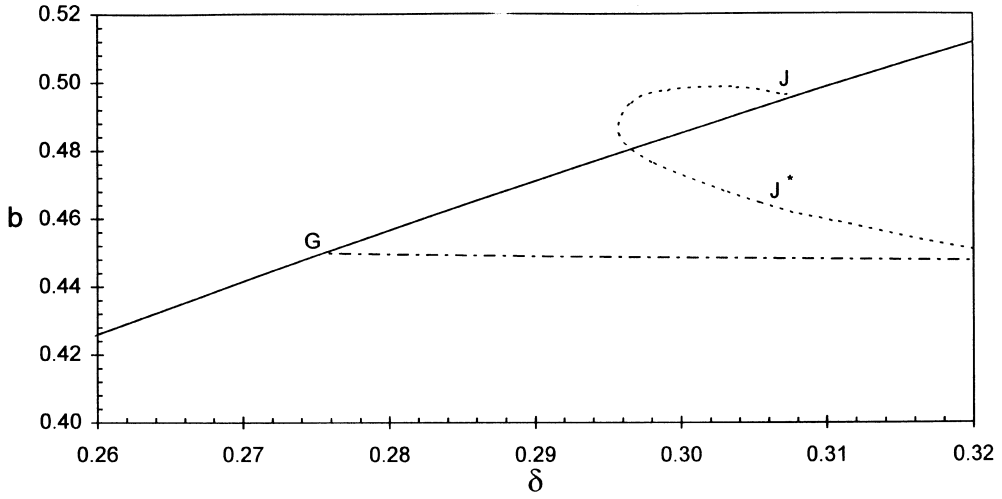

Fig. 13. Effect of downward displacement on contact length near bifurcation points G and J for $c = 0.6$.

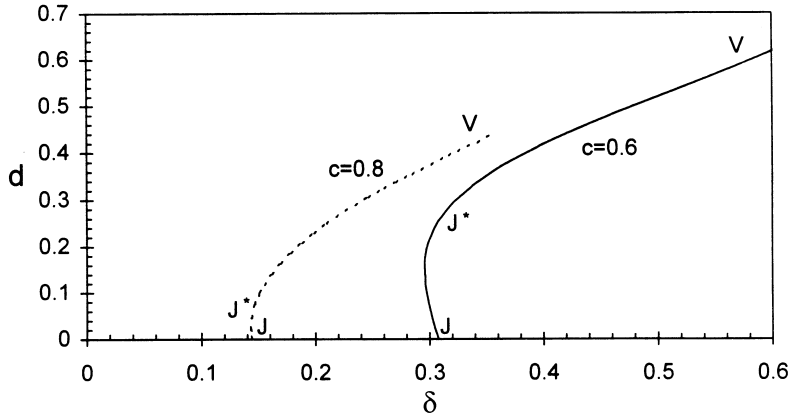

Fig. 14. Effect of downward displacement on height of buckled region ($c = 0.6$ and 0.8).

variable $t(0)$ and q. For $c = 0.6$ and 0.8, the critical point is denoted J in Figs 9, 10, 13, and 14, and in Table 3.

The shape of the strip can be obtained using a shooting method. In this case the origin is placed at the center of the buckled region, so that $x = y = \theta = 0$ at $s = 0$, and $x = c$, $\theta = \pi/2$ at $s = 1$, in nondimensional terms. Equations (3a–c) and (9) are integrated numerically, with $q = 0$ in (9) until θ is zero (at the contact point). The value of q is specified and values of $m(0)$ and p are varied until the conditions at $s = 1$, are satisfied.

In some cases it is difficult to determine values of $m(0)$ and p which will lead to convergence of the shooting method, and then a solution in terms of integrals may be more convenient. In nondimensional terms, one-fourth of the buckled region can be treated as a cantilever subjected

Table 3
Bifurcation of buckled shape and symmetric line contact (J, J*)

c	point	h	δ	b	q	p	m_o
0.6	J	0.361	0.308	0.495	67.7	40.2	−7.42
0.6	J*	0.361	0.308	0.461	33.3	36.3	−3.89
0.8	J	0.293	0.144	0.525	36.0	35.8	−0.582
0.8	J*	0.293	0.144	0.538	33.7	33.9	−0.330

to a horizontal load p. The solution for the buckled region can be expressed in terms of complete elliptic integrals of the first kind, $K(k)$, and the second kind, $E(k)$, where $0<k<1$ (Timoshenko and Gere, 1961). One obtains the relationships

$$b = 2[2E(k)-K(k)]/\sqrt{p}, \quad r = 2K(k)/\sqrt{p}, \quad m_b = 2k\sqrt{p}, \quad d = 4k/\sqrt{p} \quad \text{(13a,b,c,d)}$$

where r and m_b are the values of s and the bending moment, respectively, at the right contact point, and d is the nondimensional height of the buckled region, defined in eqn (2) where D is the dimensional height.

For the region between the right contact point and right end, if there is no inflection point, one can show that

$$1-r = \int_0^{\pi/2} \rho \, d\theta, \quad c-b = \int_0^{\pi/2} \rho \cos\theta \, d\theta \qquad \text{(14a,b)}$$

where

$$\rho = 1/\sqrt{2(p\cos\theta - p + q\sin\theta + 0.5m_b^2)}. \qquad (15)$$

With the use of eqns (13a–c, 15), (14a, b) can be written in terms of c, k, p, and q. Then one can specify two of these parameters (such as c and p, or c and q) and solve numerically for the remaining two. If there is an inflection point [as in Fig. 2(c)], the right-hand sides of eqns (14a, b) are replaced by the right-hand sides of eqns (7a, b), respectively, then a third equation is obtained by setting the denominator in eqn (15) equal to zero at $\theta = \alpha$ (the inflection point), and the three equations are solved numerically with α being an additional unknown parameter. The height h can be computed from the right-hand side of eqn (7c), and the moment m_o at the support can be obtained from equilibrium. The outer regions have inflection points if $m_o<0$, which occurs for $c = 0.6$ if $\delta<0.397$ and for $c = 0.8$ if $\delta<0.149$.

The variations of b, m_o, q, and p with δ for $c = 0.6$ and 0.8 are plotted as the dotted curves JV in Figs 9 and 10, respectively. The behavior near the bifurcation point in Fig. 9 is expanded in Fig. 13. In addition, the variation of the nondimensional buckled height d along the curves JV is shown in Fig. 14. The central region can deflect higher than the ends of the strip (i.e., d can be larger than h). This occurs when δ becomes greater than 0.338 for $c = 0.6$ and 0.203 for $c = 0.8$.

The dotted curves JV in Figs 9 and 10 bifurcate in the direction of smaller values of δ at J, and then turn around toward larger values of δ (see Fig. 13). This means that if the strip is in a

Table 4
Formation of two loops in symmetric line contact

c	h	δ	b	b_{loop}	q	p	m_{o}
0	0.0641	0.785	0.240	0.167	65.2	−29.7	−17.6
0.2	0.0512	0.794	0.392	0.134	102	−46.4	−22.0
0.4	0.0384	0.751	0.544	0.100	181	−82.5	−29.3
0.6	0.0256	0.643	0.696	0.0668	408	−186	−43.9
0.8	0.0128	0.424	0.848	0.0334	1630	−742	−87.8

symmetric, flattened equilibrium shape when it reaches J, the transition to the buckled shape is not smooth and there is a sudden snap to point J* (see Figs 13 and 14). For $c = 0.6$ and 0.8, respectively, the central deflection jumps to a height of $d = 0.253$ and 0.0445, and the values of the other parameters at J* are listed in Table 3. It is seen that q, p, and $|m_{\text{o}}|$ decrease suddenly when the elastica snaps, whereas b decreases if $c = 0.6$ and increases if $c = 0.8$.

Equilibrium configurations with the form shown in Fig. 2(d) also may exist if c is sufficiently small. The two sides of the buckled region come into contact at a point (self-contact). The portion between the two surface contact points is the same as that for a compressed buckled elastica with clamped ends (Flaherty and Keller, 1973). To analyze shapes of this type, the similarity solution eqn (8) is used for the central loop, and an integral solution is applied to the remaining length. There is no vertical force component in the segments between the surface contact points and the self-contact point, and the horizontal component is smaller in the loop than in the rest of the strip due to the force at the point of self-contact (except for the initiation of self-contact, when the nondimensional horizontal force in the loop is also equal to p). Figure 2(d) depicts the shape for this initiation when $c = 0.2$, with $h = 0.0478$, $\delta = 0.797$, $q = 272$, $p = 21.7$, and $m_{\text{o}} = 23.7$.

6. Symmetric with two loops

Equilibrium shapes such as the one depicted in Fig. 2(e) may exist if the strip is pushed down sufficiently far. The upper part of the strip makes contact with the flattened part (on the surface) at two points.

To find the equilibrium solutions for this form, a similarity solution given by Wang (1981) is utilized for the loops. If Q_2 denotes the reaction force at each end of the contact region, then in nondimensional terms

$$p = -0.45532q_2, b_{\text{loop}} = 1.34954/\sqrt{q_2},$$
$$s_{\text{u}} = 5.26292/\sqrt{q_2}, m_{\text{b}} = 1.34954\sqrt{q_2} \tag{16}$$

where $q_2 = \text{Q}_2L^2/(EI)$, b_{loop} is the contact length of each loop, s_{u} is the arc length of the uplifted part of each loop, and m_{b} is the bending moment for the upper part of the strip at the contact point. The shape between the clamped ends and the contact points can be determined using either a shooting method or an integral formulation.

Table 4 lists the minimum values of δ at which this type of shape can exist for $c = 0$, 0.2, 0.4,

0.6, and 0.8, along with corresponding values of other parameters ($2b$ is the total contact length). The values of δ are outside the ranges plotted in Figs 6–10. Figure 2(e) is associated with the case $c = 0.2$ in Table 4.

7. Asymmetric equilibrium shapes

Asymmetric equilibrium configurations are possible. Three types are illustrated in Figs 2(f), (g), and (h). When an asymmetric shape exists, the mirror image also exists. Figure 15 depicts the coordinate systems and forces used in the analysis for the cases in Figs 2(f) and (g), with $B = 0$ in Fig. 2(f). The notation and nondimensionalization are similar to those used before, except that subscripts are added when appropriate.

First, the case of point contact is considered (Fig. 2(f)). Either a shooting method or integral formulation can be used to obtain solutions. If c is sufficiently small, bifurcation occurs from a shape with symmetric point contact to asymmetric shapes with point contact. Results for $c = 0$ and 0.2 are plotted as dash-dot segments GW in Figs 6 and 7, respectively, with G denoting the bifurcation point. The parameters at G are listed in Table 5. Figure 2(f) corresponds to the case $c = 0.2$, $h = 0.390$, $\delta = 0.455$, $q_1 = 3.10$, $q_2 = 28.6$, $p = -3.37$, $m_{o1} = 3.60$, and $m_{o2} = -7.99$.

Next, asymmetric configurations with line contact are treated (Figs 2(g) and 15). A shooting method is used to obtain solutions. There are ten first-order equations, given by eqns (11a–e) with subscripts 1 and then 2 added to all quantities except p and z. The scaled arc length z varies from 0 to 1 on both uplifted segments. The known initial conditions at $z = 0$ are $x_1 = y_1 = \theta_1 = m_1 = x_2 = y_2 = \theta_2 = m_2 = 0$. Values of c and p are specified, and values of $t_1(0)$, $t_2(0)$, q_1, and q_2 are varied until the following conditions are satisfied at $z = 1$: $\theta_1 = \pi/2$, $\theta_2 = \pi/2$, $y_1 = y_2$, and $x_1 + x_2 - t_1 - t_2 = 2(c-1)$. (This last condition is derived by eliminating b in the two relations $x_1 + x_2 + 2b = 2c$ and $t_1 + t_2 + 2b = 2$ governing horizontal and arc lengths.) In Fig. 15, M_{o1} as drawn is the negative of M_1 at the left end, due to the orientation of the coordinate system.

A solution in terms of integrals is utilized when appropriate initial guesses for shooting cannot be found easily. It is assumed that the strip has an inflection point on the right part when $\theta = \alpha$, but not on the left part. The values of s_1, x_1, and y_1 at the left end, denoted s_L, x_L, and y_L, are given by the integrals of ρ, $\rho\cos\theta$, and $\rho\sin\theta$, respectively, from $\theta = 0$ to $\theta = \pi/2$, where ρ is given by (12) with q replaced by q_1. The values of s_2, x_2, and y_2 at the right end, denoted by s_R, x_R, and y_R,

Table 5
Bifurcation of symmetric and asymmetric shapes (G)

c	h	δ	b	q	p	m_o
0	0.819	0.0292	0	6.66	9.20	−3.43
0.2	0.770	0.0751	0	12.5	9.00	−3.01
0.4	0.589	0.200	0.175	22.9	15.4	−3.89
0.6	0.393	0.275	0.450	51.6	34.6	−5.83
0.8	0.188	0.249	0.737	238	150	−13.2

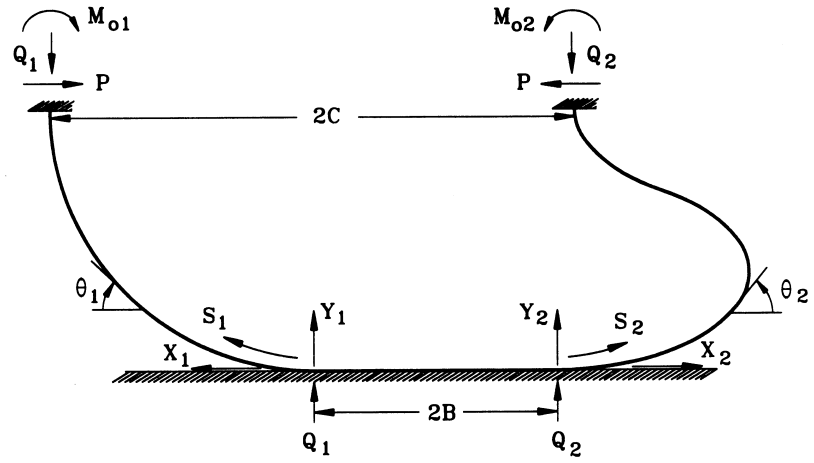

Fig. 15. Geometry of strip for asymmetric shape with line contact.

are given by the right sides of eqns (7a, b, c), respectively where ρ is given by (12) with q replaced by q_2. Based on equal heights of the ends, the given separation length and arc length, and zero bending moment at $\theta = \alpha$, there are three conditions,

$$y_L = y_R, \quad s_L + s_R + 2c = x_L + x_R + 2, \quad p\cos\alpha - p + q_2 \sin\alpha = 0 \tag{17a,b,c}$$

involving α, p,q_1, and q_2. One of these parameters is specified, and eqns (17a, b, c) are solved numerically for the remaining three.

In Figs 6 and 7 (with $c = 0$ and 0.2, respectively), the asymmetric shapes change from point contact to line contact at W. The curves ending at N_1 correspond to the side of the strip with the shorter uplifted arc length (i.e., the left side in Fig. 15), and N_2 to the other side. Parameters at W for $c = 0$ and 0.2 are listed in Table 6. Figure 2(g) depicts the configuration for $c = 0.2$, $h = 0.189$, $\delta = 0.656$, $b = 0.214$, $q_1 = 15.0$, $q_2 = 29.1$, $p = -10.3$, $m_{o1} = 7.12$, and $m_{o2} = -8.88$.

For $c = 0.4$, 0.6, and 0.8, in Figs 8, 9, and 10, respectively, bifurcation occurs from symmetric line contact to asymmetric line contact at G. The parameters at this point are given in Table 5. As δ is increased past its value at G, the asymmetric contact length first decreases slightly and then increases, as shown on the dash-dot path GN in part (a) of Figs 8–10.

If $c > 0$ and the strip is pushed down sufficiently far in an asymmetric shape, the upper part of the strip on one side will contact the surface, as depicted in Fig. 2(h). The similarity solution in

Table 6
Transition from asymmetric point contact to asymmetric line contact (W)

c	h	δ	q_1	q_2	p	m_{o1}	m_{o2}
0	0.252	0.596	8.16	18.7	−6.34	5.39	−7.08
0.2	0.384	0.462	3.16	28.6	−3.58	3.67	−8.03

Table 7
Formation of loop in asymmetric line contact

c	h	δ	b	b_{loop}	q_1	q_2	p	m_{o1}	m_{o2}
0.2	0.099	0.746	0.301	0.259	66.6	27.2	−12.4	12.6	−11.3
0.4	0.075	0.715	0.476	0.194	118	48.3	−22.0	16.7	−15.1
0.6	0.049	0.619	0.690	0.129	266	109	−49.5	25.1	−22.7
0.8	0.025	0.412	0.825	0.0647	1065	435	−198	50.2	−45.3

eqn (16) is utilized to analyze the loop, and a shooting method or integral formulation is applied to the other uplifted segments. For $c = 0.2$, 0.4, 0.6, and 0.8, this form occurs first at the values of δ given in Table 7, along with the other listed parameters ($2b$ is the total contact length). These points are out of the ranges in Figs 7–10. The shape in Fig. 2(h) corresponds to the case $c = 0.2$ in Table 7.

The case $c = 0$, in which the ends of the strip are clamped together, deserves special attention. Figure 16 illustrates three equilibrium shapes. When δ reaches the value 0.668, shown in Fig. 16(a), the curvatures at the ends of the upper and lower portions of the strip become identical. The other parameters at this stage (which is beyond the range of Fig. 6) are $h = 0.181$, $b = 0.074$, $q_1 = q_2 = 18.3$, $p = -7.54$, and $m_{o1} = -m_{o2} = 7.19$, where the forces and moments are measured just below the clamped end.

As the strip is pushed down further, a contact region is formed between the upper and lower portions. Figure 16(b) depicts the case $\delta = 0.688$, $h = 0.161$, $b = 0.0926$, $q_1 = 18.4$, $q_2 = 19.3$, $p = -8.60$, and total moment $m = 14.4$ at the end. Contact occurs between the clamped end and the leftmost tick mark. In this region, the effective bending stiffness is doubled, so that the left side

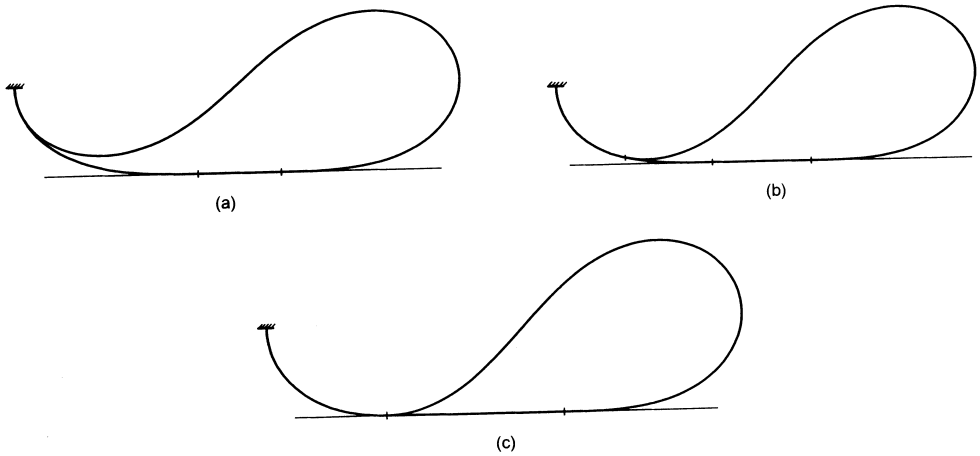

Fig. 16. For $c = 0$, equilibrium shapes when upper and lower portions: (a) have same curvature at clamped end; (b) are in contact for a region near the end; (c) are in contact from the end to the surface.

of (3c) is multiplied by the factor 2. The shooting procedure involves three sets of equations of the form (11a–e), with arc lengths starting at the two lift-off points and the clamped end.

Finally, if δ is sufficiently high, the upper and lower portions of the strip are in contact from the clamped end to the surface, as in Fig. 16(c). Equations (16) are applied for the loop. The given total arc length leads to the condition

$$s_u + b_{loop} + 2\int_0^{\pi/2} \rho \, d\theta = 2 \tag{18a}$$

where

$$\rho = 1/\sqrt{(q_1 + q_2)\sin\theta + 0.25m_b^2}. \tag{18b}$$

The right reaction force q_2 is specified, then s_u, b_{loop}, and m_b are computed from eqn (16), and then eqn (18a) is solved numerically for the left reaction force q_1. In Fig. 16(c), $\delta = 0.692$, $h = 0.156$, $b = 0.147$, $q_1 = 22.0$, $q_2 = 20.9$, and the total moment at the clamped end is $m = 14.5$.

8. Concluding remarks

Some interesting planar equilibrium shapes have been demonstrated for a thin, inextensible, elastic strip that is bent and then pushed down onto a flat surface. First the equilibrium shape for the bent elastica was determined for various separation distances between the clamped ends (Fig. 1). Then the strip was pushed down onto a flat surface, and various equilibrium configurations were obtained (Fig. 2). Both symmetric and asymmetric shapes are possible, and cases with point contact, line contact, buckling of a central region, and one or two loops may occur.

The problem involves displacement control (Bazant and Cedolin, 1991), and the results depend on the nondimensional downward displacement δ of the clamped ends. As the bent strip is pushed down on the surface, the initial shape is symmetric and there is contact only at the central point of the strip [Fig. 2(a)]. With the use of Fig. 5, symmetry, and eqn (2), the total potential U of the strip in this shape can be written in nondimensional terms as

$$u = \int_0^1 \left(\frac{d\theta}{ds}\right)^2 ds + 2q\int_0^1 \sin\theta \, ds + 2p\int_0^1 \cos\theta \, ds. \tag{19}$$

As δ is increased from zero, u has a local minimum initially, and this symmetric point-contact configuration is stable initially.

If the nondimensional separation distance between the clamped ends is $c = 0.2$, the symmetric form with point contact becomes unstable when the bifurcation point G in Fig. 7 is reached. Upon further increase of δ, this state becomes unstable and the strip moves to the left or right into an asymmetric configuration with point contact [Fig. 2(f)]. At W in Fig. 7, the curvature of the strip at the contact point vanishes, and thereafter a flat contact region (line contact) exists [Fig. 2(g)]. With further downward displacement, the upper portion of the strip makes contact with the lower portion, forming a loop [Fig. 2(h)].

For $c = 0.4$ and 0.6, the symmetric form with point contact flattens into a symmetric shape with line contact [Fig. 2(b)] at point F in Figs 8 and 9, respectively, before the bifurcation point G is

reached. These shapes are stable until point G, after which the strip slides into an asymmetric configuration with line contact. If the strip is pushed down further, a loop is formed when δ becomes sufficiently large, as for $c = 0.2$.

Results for $c = 0.8$ are presented in Fig. 10. Symmetric configurations with point contact and then line contact are stable until the bifurcation point J is reached. Upon further increase of δ, the flattened portion of the strip snaps into a buckled shape [Fig. 2(c)], and the height of the buckled region increases.

Figure 6 depicts equilibrium paths for the case $c = 0$, when the ends of the strip are held together. The symmetric shape with point contact is stable until G is reached, and then the strip takes on an asymmetric shape with point contact which spreads into line contact at W. As δ is increased further, the two ends of the strip take on the same curvature [Fig. 16(a)] and then come into contact over a region [Fig. 16(b)] which enlargens until it reaches the flat surface [Fig. 16(c)].

The analysis in this paper has assumed that there is no friction between the elastica and the surface. If friction is present, the behavior may be different than just described. For example, if $c = 0$, 0.2, or 0.4 (Figs 6–8), the strip may remain symmetric and not move into an asymmetric shape, and then may exhibit the form in Fig. 2(e) with two loops. If $c = 0.6$, the configuration may remain symmetric past point G in Fig. 9 and then the central region will buckle when point J is reached. Friction may also cause the flattened portion of the asymmetric shape with the form in Fig. 2(g) to buckle; this was observed in an experiment, but did not occur in the numerical computations (since the nondimensional compressive load p in the asymmetric flattened region did not exceed the critical value $(\pi/b)^2$, where b is half the nondimensional contact length).

Acknowledgements

Two of the authors (D.A.D., B.E.W.) are grateful for the support of the Adhesive and Sealant Council, the Center for Adhesive and Sealant Science at Virginia Tech, and the National Science Foundation Science and Technology Center on High Performance Polymeric Adhesives and Composites (contract DMR 9120004). One of the authors (L.T.W.) is grateful for support under AFOSR Grant F49620-96-1-0089 and NSF Grant DMS-9625968.

References

Bahder, T. (1995) *Mathematica for Scientists and Engineers*. Addison-Wesley, Reading, Massachusetts.

Bazant, Z. P. and Cedolin, L. (1991) *Stability of Structures*. Oxford University Press, New York.

Evans, E. A. (1980) Analysis of adhesion of large vesicles to surfaces. *Biophysical J.* **31,** 425–432.

Evans, E. A. and Skalak, R. (1980) *Mechanics and Thermodynamics of Biomembranes*. CRC Press, Boca Raton, Florida.

Feng, W. W. and Yang, W.-H. (1973) On the contact problem of an inflated spherical membrane. *J. Appl. Mech.* **40,** 209–214.

Flaherty, J. E. and Keller, J. B. (1973) Contact problems involving a buckled elastica. *SIAM J. Appl. Math.* **24**, 215–225.

Gorski, W. (1976) A review of literature and a bibliography on finite elastic deflections of bars. *Civil Engrg. Trans., Institution of Engrs., Australia* **CE18,** 74–85.

Grigolyuk, E. I. and Shalashilin, V. I. (1991) *Problems of Nonlinear Deformation*. Kluwer, Dordrecht, The Netherlands.

Iseki, H., Sowerby, R., Bhattacharyya, D. and Gatt, P. (1989a) A theoretical and experimental study of a curved strip compressed by a flat plate. *J. Appl. Mech.* **56,** 96–104.

Iseki, H., Sowerby, R., Chandrasekaran, N. and Gatt, P. (1989b) The elastic-plastic snapping-through of a curved metal strip compressed between two rigid plates (the influence of the supported end condition on the snap-through). *JSME Int. J., I* **32,** 101–106.

Kinkead, A. N., Jennings, A., Newell, J. and Leinster, J. C. (1994) Spherical shells in inelastic collision with a rigid wall—tentative analysis and recent quasi-static testing. *J. Strain Anal.* **29,** 17–41.

Kitching, R., Houlston, R. and Johnson, W. (1975) A theoretical and experimental study of hemispherical shells subjected to axial loads between flat plates. *Int. J. Mech. Sci.* **17,** 693–703.

Mack, M. J., Jr., Gassman, P. M. and Baumgarten, J. R. (1983) Analysis of a thin-walled pressurized torus in contact with a plane. *AIAA J.* **21,** 1162–1167.

Nowinka, J. and Lukasiewicz, S. (1994) Hemisphere compressed by rigid plates. *Int. J. Non-Lin. Mechs.* **29,** 23–29.

Sugita, Y. (1985) Nonlinear load-deflection relation of toroidal shells subjected to axisymmetric compression between rigid plates. *Int. J. Mech. Sci.* **27,** 609–625.

Timoshenko, S. P. and Gere, J. M. (1961) *Theory of Elastic Stability* (2nd edn.). McGraw-Hill, New York.

Updike, D. P. and Kalnins, A. (1972) Contact pressure between an elastic spherical shell and a rigid plate. *J. Appl. Mech.* **39,** 1110–1114.

Wang, C.-Y. (1981) Folding of elastica—similarity solutions. *J. Appl. Mech.* **48,** 199–200.

Wang, C.-Y. (1987) Crushing of an elastic-perfectly plastic ring or tube between two planes. *J. Appl. Mech.* **54,** 159–164.

Wolfram, S. (1991) *Mathematica*: *A System for Doing Mathematics by Computer*. Addision-Wesley, Reading, Massachusetts.